

Enhancing immunogenic responses through CDK4/6 and HIF2 α inhibition in Merkel cell carcinoma

Jung Hyun Lee^{a,b,*}, Justin Daho Lee^b, Kelly Paulson^{a,e,f}, Valentin Voillet^d, Andre Berndt^b, Candice Church^a, Kristina Lachance^a, Song Y. Park^a, Naomi K. Yamamoto^c, Elizabeth A. Cromwell^f, Raphael Gottardo^{d,e}, Aude G. Chapuis^{a,f,g}, Paul Nghiem^{a,f,g,1}

^a Department of Dermatology, School of Medicine, University of Washington, Seattle, WA, USA

^b Institute for Stem Cell and Regenerative Medicine, University of Washington, Seattle, WA, USA

^c Medical Scientist Training Program, University of Washington, Seattle, WA, USA

^d Vaccine and Infectious Disease Division, Fred Hutchinson Cancer Research Center, Seattle, WA, USA

^e Public Health Sciences Division, Fred Hutchinson Cancer Research Center, Seattle, WA, USA

^f Seattle Cancer Care Alliance, Seattle, WA, USA

^g Clinical Research Division, Fred Hutchinson Cancer Research Center, Seattle, WA, USA

ARTICLE INFO

Keywords:

CDK4/6 inhibitor

Hypoxia

Immunogenic cell death

ABSTRACT

Approximately 50% of Merkel cell carcinoma (MCC) patients facing this highly aggressive skin cancer initially respond positively to PD-1-based immunotherapy. Nevertheless, the recurrence of MCC post-immunotherapy emphasizes the pressing need for more effective treatments. Recent research has highlighted Cyclin-dependent kinases 4 and 6 (CDK4/6) as pivotal cell cycle regulators gaining prominence in cancer studies. This study reveals that the CDK4/6 inhibitor, palbociclib can enhance PD-L1 gene transcription and surface expression in MCC cells by activating HIF2 α . Inhibiting HIF2 α with TC-S7009 effectively counteracts palbociclib-induced PD-L1 transcription and significantly intensifies cell death in MCC. Simultaneously, co-targeting CDK4/6 and HIF2 α boosts ROS levels while suppressing SLC7A11, a key regulator of cellular redox balance, promoting ferroptosis- a form of immunogenic cell death linked to iron. Considering the rising importance of immunogenic cell death in immunotherapy, this strategy holds promise for improving future MCC treatments, markedly increasing immunogenic cell death various across various MCC cell lines, thus advancing cancer immunotherapy.

1. Introduction

Merkel cell carcinoma (MCC), which also encompasses neuroendocrine skin carcinomas [1], has witnessed a fourfold increase in incidence since 1986, primarily affecting the elderly population [2]. While MCC's etiology is multifaceted, around 80% of cases are linked to the Merkel cell polyomavirus (MCPyV), with extended exposure to UV radiation responsible for the remainder, causing DNA damage [3]. There is an urgent need for effective MCC treatment strategies, particularly in light of recurrent MCC and acquired

* Corresponding author. Department of Dermatology, School of Medicine, University of Washington, Seattle, WA, USA.

E-mail address: jlee24@uw.edu (J.H. Lee).

¹ These authors contributed equally to this work.

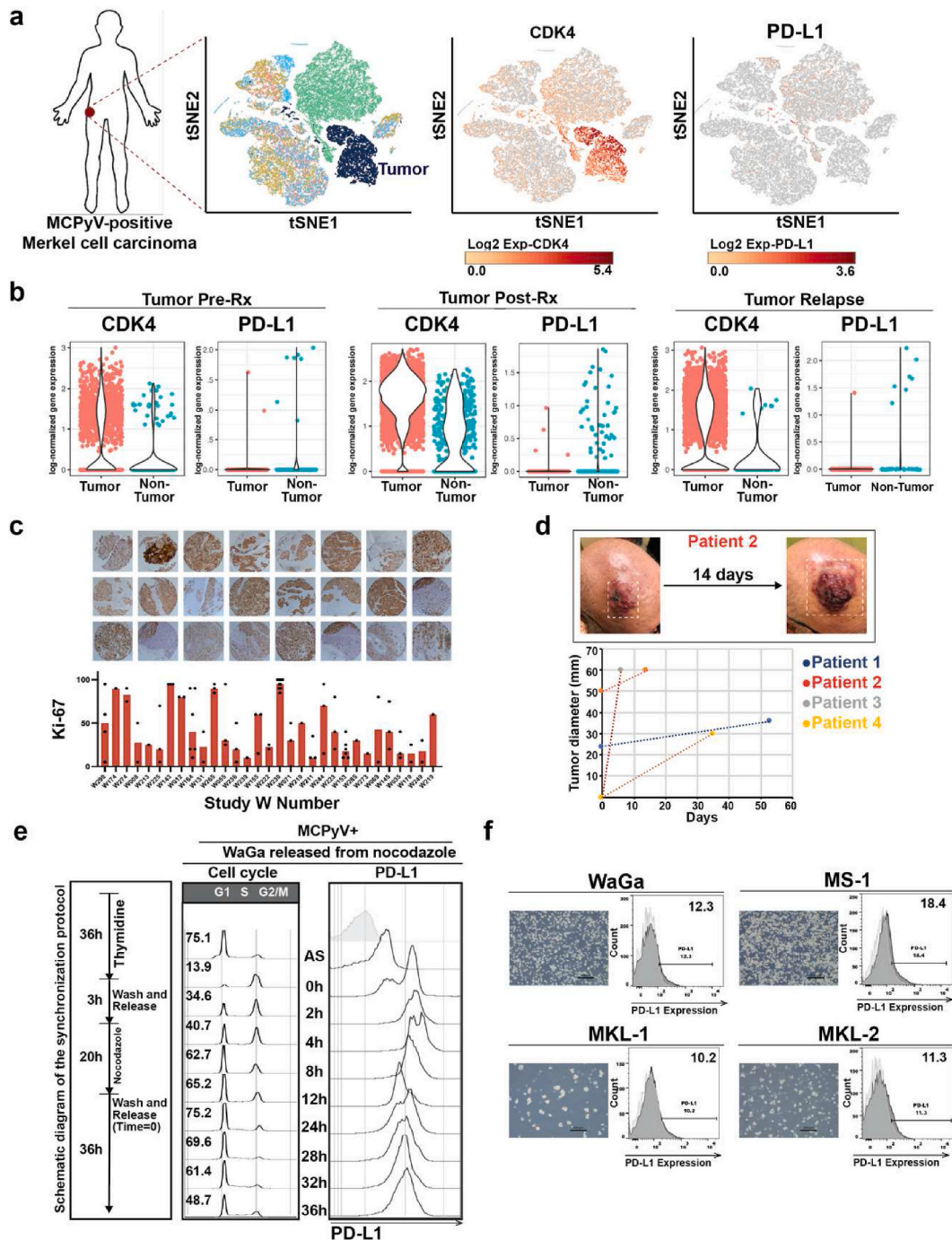


Fig. 1. Expression of CDK4 and PD-L1 in Merkel cell carcinoma. **a**, Cell clusters resolved by PCA-based t-distributed stochastic neighbor embedding (t-SNE) are shown in an aggregate analysis of paired tumor/PBMC samples. **b**, Violin plots of CDK4 and CD274 scores for Tumor-Biopsy (Bx), Pre-Rx, and Relapse samples; each dot represents one MCC cell. **c**, Representative IHC of an MCC TMA produced from 31 patient samples (top). Average Ki-67 scores across all samples from each patient (bottom). **d**, Representative clinical pictures of the rapid growth of MCC tumors. A significant increase in tumor size occurred within 14 days for a patient who received no treatment (top). Chart showing tumor size change in two months for four patients with no treatment (bottom). The average growth of tumor diameter was approximately 2 cm/week as per available data. **e**, Cell-cycle profiles and PD-L1 expression as monitored by fluorescence-activated cell sorting (FACS). **f**, Representative light micrographs of WaGa, MS-1, MKL-1, and MKL-2 cells. Dark grey histograms depict binding of anti-PD-L1 mAbs, whereas light grey histograms indicate non-stained cells.

resistance to existing therapies [4]. Recurrent MCC often establishes an immunosuppressive microenvironment that supports tumor proliferation, necessitating innovative approaches to boost treatment efficacy [1]. Immunotherapies, such as programmed death 1 (PD-1)/PD-L1 blockade, have shown remarkable effectiveness [5]. It is worth noting that Merkel cell polyomavirus (MCPyV) marked the first confirmed oncogenic polyomavirus (PyV) in humans [6]. Therefore, gaining insights into effectively targeting proteins that enhance immunotherapy for MCC is critical for improving treatment outcomes.

This study embarks on a novel approach to address the challenges of MCC treatment by investigating the combination of CDK4/6 and HIF2 α inhibitors, specifically palbociclib and TC-S7009, aiming to induce cell death in hypoxia-induced MCC. Our research seeks to enhance the efficacy of combination immunotherapy by developing complementary chemotherapy regimens capable of triggering immunogenic cell death (ICD). The dysregulated cell cycle is a fundamental driver of cancer cell proliferation, rendering proteins like CDK4/6 attractive therapeutic targets [7]. CDK4/6 inhibitors have already demonstrated their ability to halt cancer cell proliferation by inducing G1 cell cycle arrest [8]. In this context, CDK4/6 is pivotal in orchestrating the cell cycle transition from the G1 phase to the S phase [9]. As such, focusing on CDK4/6 among the CDKs is a pragmatic approach [10]. Additionally, CDK4/6 inhibitors exhibit the ability to suppress regulatory T (Treg) cell proliferation while enhancing cytotoxic T cell (CTL) activity, thereby facilitating the clearance of tumor cells [11–13].

Moreover, MCC often experiences hypoxia due to its rapid growth and heightened oxygen consumption, contributing to unfavorable clinical outcomes. Hypoxia-induced cell death, notably immunogenic cell death (ICD), has emerged as a promising avenue to enhance immunotherapy [14]. Understanding the mechanisms by which chemotherapy can trigger ICD is pivotal in advancing the concept of combination immunotherapy as an innovative cancer treatment strategy. Hypoxia-inducible factors (HIFs), frequently overexpressed in tumor cells, assume crucial roles in cancer cell survival, therapy resistance, and recurrence [15]. Recent attention has been directed towards targeting HIFs, particularly HIF-2 α , to improve treatment outcomes in metastatic and treatment-resistant cancers [16].

Furthermore, when mitochondria are affected by CDK4/6 inhibitors, they can increase the production of reactive oxygen species (ROS). Tumor cells often encounter hypoxia due to their rapid proliferation and heightened oxygen consumption, resulting in tumor heterogeneity and unfavorable clinical outcomes [17]. Chemotherapy-induced ICD holds the potential to stimulate immune responses, releasing tumor antigens and inducing immunogenic modulation to enhance ICD [18]. HIFs centrally regulate the expression of critical genes for cell survival, significantly influence the characteristics of cancer cells, and contribute to chemotherapy and radiotherapy resistance, poor prognosis, and tumor recurrence [19]. Recently developed HIF-2 α inhibitors have exhibited promising effectiveness and safety profiles in clinical trials. In light of these considerations, this study explores the potent combination treatment of CDK4/6 and HIF2 α inhibitors, namely palbociclib and TC-S7009, to induce cell death in hypoxia-induced MCC. This research aims to enhance the effectiveness of combination immunotherapy by formulating complementary chemotherapy regimens capable of triggering ICD.

2. Results

2.1. The expression pattern of PD-L1 during the cell cycle of Merkel cell carcinoma

Immunotherapy, remarkably immune checkpoint inhibitors like PD-1 and PD-L1 blockers, has shown promise in treating Merkel cell carcinoma (MCC), particularly in cases of advanced disease. These drugs disrupt communication between immune cells and cancer cells, enabling the immune system to target and eliminate cancer cells.

To investigate MCC's rapid growth and immunogenic characteristics, we used single-cell RNA (scRNA) sequencing data from tissue samples of patients who exhibited late/acquired resistance [4]. Our analysis revealed significant differential expression of cell cycle genes, notably CDK4 and the immune checkpoint PD-L1. CDK4 consistently exhibited high expression levels in tumor samples across all cases, both before and after immunotherapy, as well as upon relapse, while PD-L1 levels remained low (Fig. 1a and b).

We performed Ki-67 staining on tissue microarrays (TMA) containing 31 MCC tumors to further explore MCC's rapid growth characteristics. The results showed a median Ki-67 positivity rate of 67% in tumor cells, indicating a very high rate of cellular proliferation (Fig. 1c). As depicted in Fig. 1d (upper panel), we observed a striking case illustrating the rapid growth of MCC tumors, where the size of a tumor mass on the head of a Caucasian male significantly increased over just two weeks. Moreover, charts displaying changes in diameter sizes for four tumors demonstrated rapid growth in multiple cases within a short timeframe, as showed in Fig. 1d (lower panel).

The immune checkpoint PD-L1 is expressed on the surface of various tumor cells and plays a role in immunosuppression, allowing tumors to evade the host's anticancer surveillance [20]. PD-L1, belonging to the immunoglobulin superfamily [21], has proven to be a valuable biomarker in various cancer types [22]. Our study observed that a representative MCPyV-positive MCC cell line exhibited deficient PD-L1 expression (Fig. 1e), consistent with previous reports [23].

We further examined PD-L1 expression throughout different cell cycle phases, following established protocols from prior studies [13,24,25].

We synchronized MCPyV-positive WaGa cell lines by inducing G2/M phase arrest through a thymidine-nocodazole double block and subsequently analyzed PD-L1 expression levels using flow cytometry as the cell cycle progressed. In this context, PD-L1 exhibited a fluctuating pattern, gradually increasing as cells advanced through the G2/M phase and decreasing as they passed through the G1 phase, as depicted in Fig. 1e. The dynamic expression pattern of PD-L1 across cell cycle phases helps explain the high CDK4 expression and low PD-L1 expression observed in WaGa cells.

Our investigation of PD-L1 expression in other MCPyV-positive MCC cell lines, such as MS-1, MKL-1, and MKL-2, revealed similarly low expression levels consistent with the WaGa cell line (Fig. 1f). Following synchronization through a thymidine double block, we

also examined the PD-L1 expression pattern in HeLa and MCPyV-negative MCC13 cells. This pattern, akin to that observed in WaGa cells, showed an increase during the G2/M phase and a decrease during the G1 phase (Extended Data Fig. 1a–c). In summary, the immune therapy target PD-L1 undergoes dynamic regulation closely linked to the cell cycle in MCC.

2.2. Palbociclib CDK4/6 inhibitor induces PD-L1 upregulation in virus-positive MCC cells

The dysregulation of CDK4/6 significantly contributes to abnormal cell cycle progression, particularly in cancer [7]. Serine/threonine and tyrosine kinases present appealing therapeutic targets due to their close correlation with tumor cell proliferation [26–28]. This has led to the development of small-molecule kinase inhibitors [12], which have proven to be effective, non-toxic, and attractive components for anticancer therapy [11]. The FDA-approved small molecule targeting CDK4/6, Palbociclib, has demonstrated efficacy in numerous clinical trials [29]. We treated virus-positive MCC cell lines with Palbociclib and observed its effects on PD-L1 expression and cell viability. According to flow cytometry analysis, Palbociclib treatment resulted in a dose-dependent increase in PD-L1 protein levels in MCPyV-positive MCC cells WaGa, MS-1, MKL-1, and MKL-2, in contrast to the control group treated with

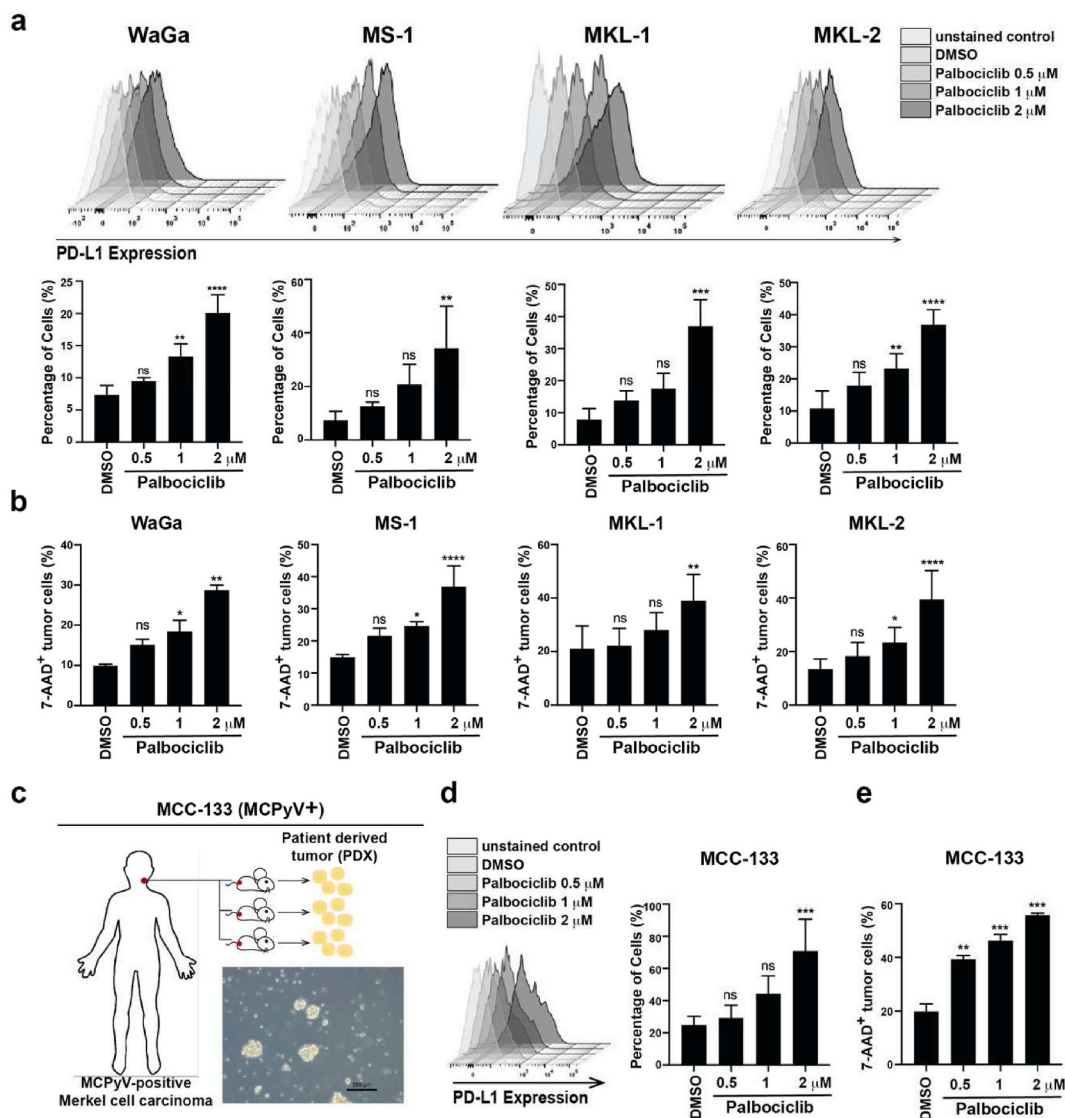


Fig. 2. Palbociclib, a selective inhibitor of CDK4/6, increases the protein level of PD-L1 and reduces the viability of Merkel cell carcinoma tumor cells. **a**, FACS analysis of cell surface expression of PD-L1 in WaGa, MS-1, MKL-1, and MKL-2 cells **b**, Percentage of 7-AAD⁺ dead MCC cells after treating with palbociclib for 72 h **c**, Schematic illustrating the generation of patient-derived xenograft (PDX) model. Tumor specimens obtained from consented patients were processed and implanted subcutaneously into 5-week to 6-week-old immunodeficient mice. During the initial engraftment phase, tumors were allowed to establish and grow for three to six months. **d**, Representative histograms showing PD-L1 expression in cell lines when treated with the indicated doses of Palbociclib. **e**, Percentage of 7-AAD⁺ dead PDX cell after treatment with palbociclib for 72 h.

DMSO (Fig. 2a). It is known that the immunosuppressive function of PD-L1 can impact the efficacy of chemotherapy agents that induce cell death [30–33]. PD-L1 interacts with the PD-1 receptor on the surface of T cells, inhibiting T cell activation and weakening T cell-mediated immunity [20,34,35]. This protective mechanism of cancer cells from host anti-tumor immunity significantly reduces the efficacy of many anticancer therapies, ultimately resulting in unfavorable clinical outcomes [36]. In an effort to better characterize related PD-L1 biology [24,37–40], we investigated the impact of Palbociclib on the immune microenvironment and the survival of virus-positive MCC cells. We examined the impact of palbociclib on the two principal T-antigen gene products of MCPyV [41], namely large T antigen (LT) and small T antigen (sT) [6,42,43]. MCPyV LT and sT are multifunctional proteins known to play a role in tumor formation [44–46]. Knockdown of T Antigens halts the uncontrolled cell cycle by modulating the Rb-E2F pathway [47,48].

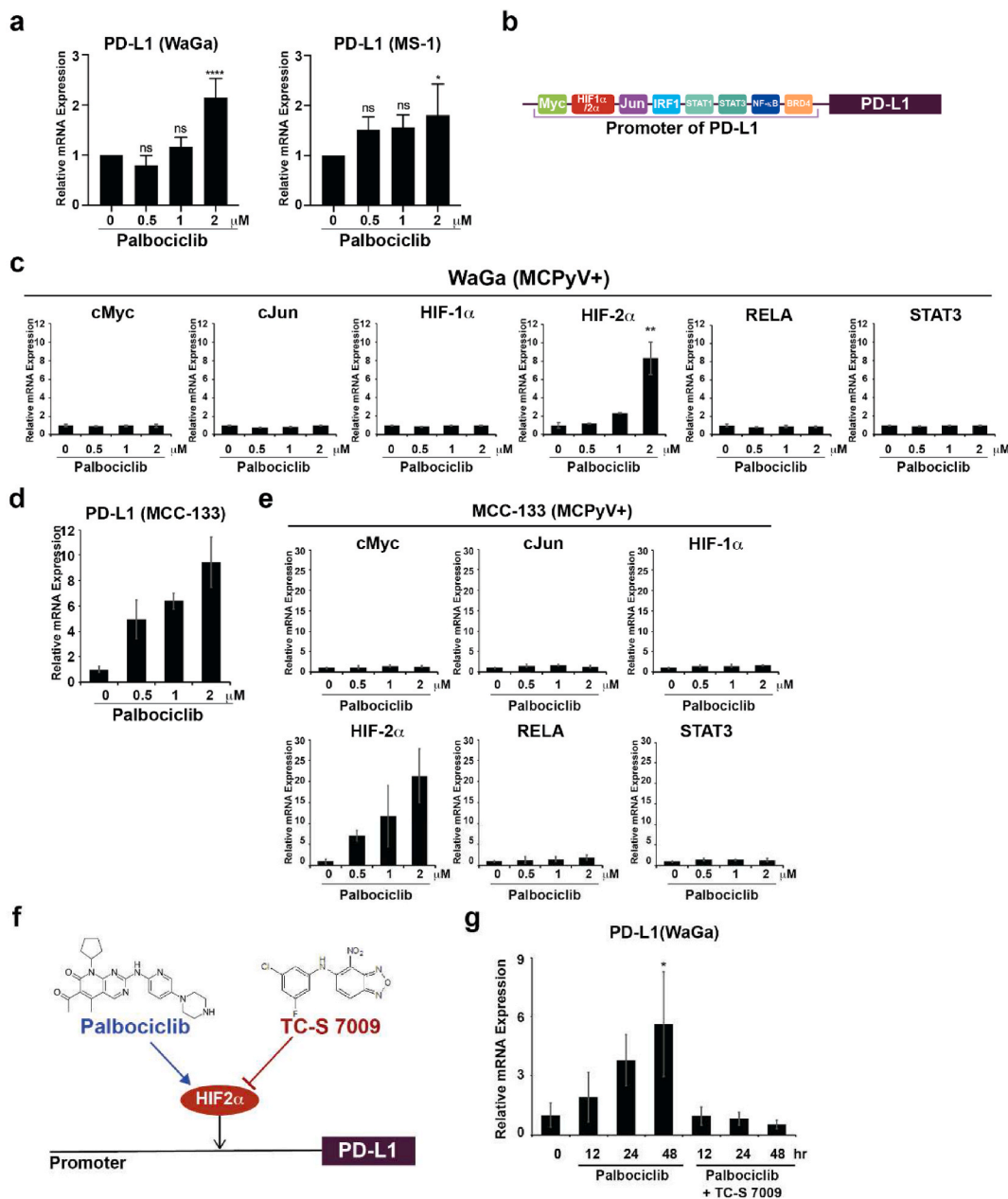


Fig. 3. Palbociclib treatment increases PD-L1 transcription via transcriptional activator HIF2α. **a**, PD-L1 mRNA levels after palbociclib treatment, as quantitated by real-time RT-PCR. **b**, Schematic illustration of TFs that bind to the promoter of the PD-L1 gene. **c**, qRT-PCR analysis of MYC, JUN, HIF1α, HIF2α, RELA, and STAT3 mRNA levels in WaGa cells treated with different doses of Palbociclib for 48 h. **d**, Quantitation of PD-L1 mRNA levels by qRT-PCR in MCC PDX cells. **e**, Quantitation of MYC, JUN, HIF1α, HIF2α, RELA, and STAT3 mRNA levels by qRT-PCR in MCC PDX cells, MCC-133. **f**, Schematic illustration of TC-S 7009 as HIF2α inhibitor. **g**, Quantitation of PD-L1 mRNA levels by qRT-PCR in WaGa cells treated with palbociclib alone or in combination with the HIF2 α inhibitor TC-S 7009 for 48 h.

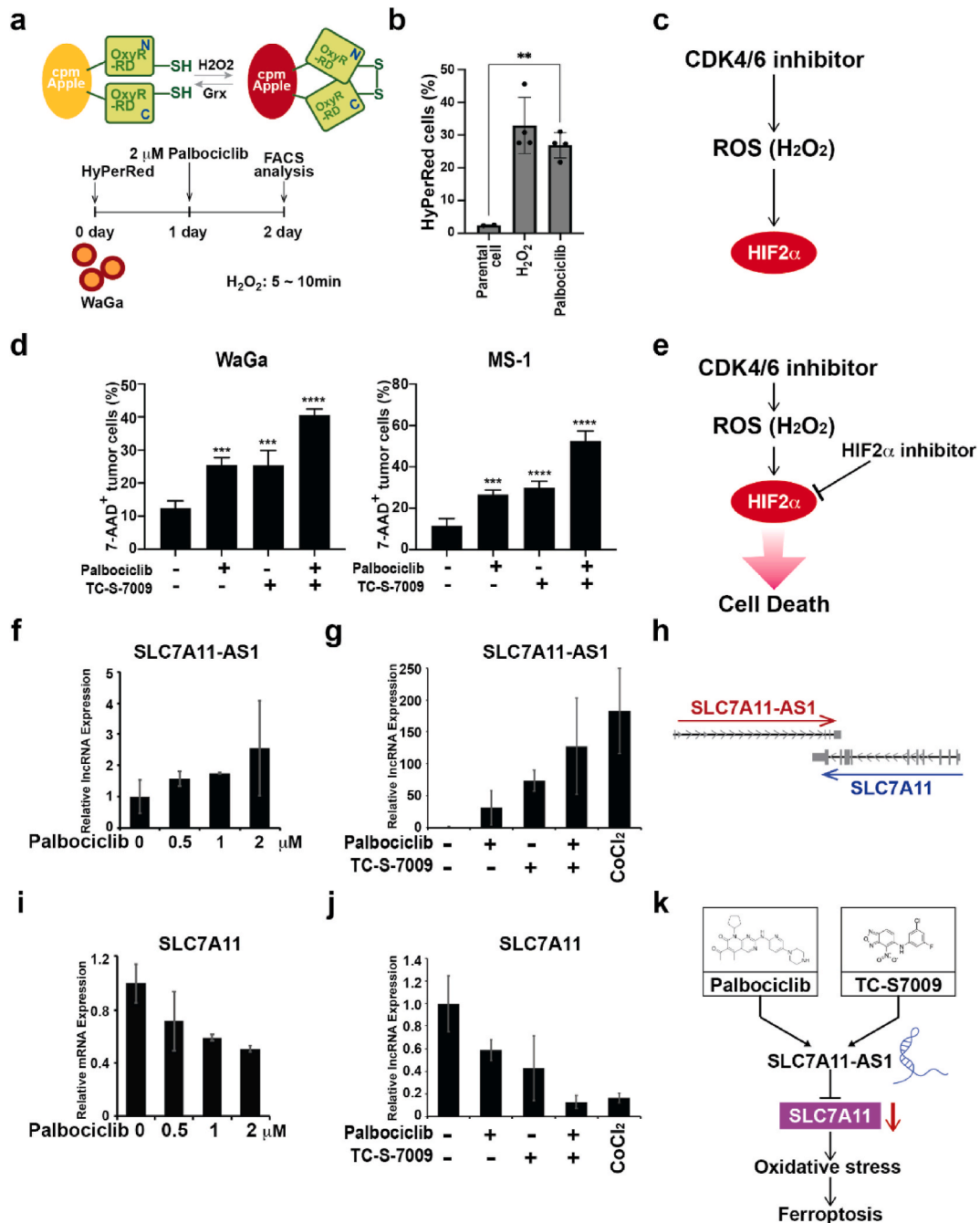


Fig. 4. Co-treatment of palbociclib and TC-S 7009 shows more potency in killing MCC tumor cells by acting via the lncRNA SLC7A11-AS1. **a**, HyPer family probe (top) and HyPerRed plasmid were transfected into WaGa cells, and intracellular H₂O₂ was measured by FACS analysis (bottom). **b**, HyPerRed transfected WaGa cells were treated with Palbociclib (2 μM) and RFP signal was quantitated by flow cytometry. H₂O₂ was used as a positive control. **c**, Simplified schematic showing the action of palbociclib and ROS (H₂O₂) on HIF2 α . **d**, The percentage of 7-AAD⁺ cells among WaGa or MS-1 cells treated with palbociclib (2 μM) and TC-S 7009 (1 μM) alone or together for 72 h. **e**, Simplified schematic as in **c** with TC-S 7009 leading to cell death. **f**, SLC7A11-AS1 lncRNA levels assessed by qRT-PCR with palbociclib treatment as indicated concentration. **g**, SLC7A11-AS1 lncRNA was measured by qRT-PCR in WaGa cells treated with palbociclib and TC-S 7009, either alone or together for 72 h. CoCl₂ was used as a control artificial hypoxia condition. **h**, Schematic illustration of SLC7A11-AS1 and SLC7A11 on the chromosome. **i**, SLC7A11 was quantitated by qRT-PCR after palbociclib treatment. **j**, SLC7A11 lncRNA was quantitated by qRT-PCR after treating with palbociclib and TC-S 7009, either alone or together for 72 h. CoCl₂ was used as a control to represent hypoxia conditions. **k**, Schematic depicting co-treatment of palbociclib and TC-S 7009 is more effective in inducing cell death by ferroptosis via SLC7A11-AS1-mediated inhibition of SLC7A11 and inducing oxidative stress.

Interestingly, treatment with palbociclib resulted in increased levels of LT and sT (Extended Data Fig. 2a and b). The alterations in LT and sT expression are considered pivotal in MCC growth. Therefore, the observed elevation of LT and sT subsequent to palbociclib-induced cell growth inhibition appears to mirror a compensatory mechanism for cell survival, akin to what is observed with PD-L1. We investigated palbociclib-induced cell death across four cell lines using 7-AAD staining and flow cytometric analysis [49]. As shown in Fig. 2b, it demonstrated a dose-dependent reduction in viable cells, allowing us to accurately quantify the impact of palbociclib on cell survival capacity. Given the lack of a transgenic mouse model for MCPyV-positive MCC, we employed a patient-derived xenograft (PDX) model, referred to as MCC-133 (Fig. 2c), in this study. Remarkably, our results from the MCC-133 PDX model were consistent with those from other cell lines, as palbociclib treatment led to an elevation in PD-L1 levels (Fig. 2d) and heightened cell death (Fig. 2e), highlighting that palbociclib induced cell death even in MCC cells derived from patients.

2.3. Palbociclib treatment induces an upregulation of HIF2 α gene expression

PD-L1 expression is subject to alterations at both transcriptional and post-translational levels and exhibits variation across different tumor types [50,51]. Several oncogenic signaling-activated transcription factors (TFs) modulate PD-L1 expression at the transcriptional level [15,52,53], and specific anticancer chemotherapeutic agents impact PD-L1 transcription [37,54]. Post-translationally, studies suggest that CDK4 and GSK3B regulate PD-L1 protein stability and degradation [38,53,55,56]. Understanding the significance of PD-L1 in cancer is crucial as the use of immune checkpoint inhibitors continues to expand, aiding in fine-tuning cancer immunotherapy strategies and solidifying its role as a predictive marker [57–59].

Following palbociclib treatment, we observed an increase in PD-L1 protein levels and conducted further investigations into whether palbociclib induces PD-L1 transcription. Our qRT-PCR analysis (Fig. 3a) demonstrated a significant upregulation of PD-L1 mRNA expression. To gain a more comprehensive understanding of PD-L1 gene upregulation, we explored the impact of palbociclib on six known transcription factors associated with the PD-L1 gene, including cMyc [60], cJun, HIF-1 α , HIF-2 α , RELA, and STAT3 [37] (Fig. 3b). Our observations revealed a substantial and noteworthy upregulation of hypoxia-inducible factor-2 α (HIF-2 α) in response to palbociclib treatment. At the same time, the expression levels of the other five candidate transcription factors remained minimally changed (Fig. 3c). These findings strongly suggest that HIF-2 α plays a specific and pivotal role in mediating the palbociclib-induced upregulation of PD-L1. Importantly, this phenomenon was observed in MCPyV-positive MCC cell lines. In contrast, an MCPyV-negative MCC cell line (MCC13) did not exhibit an increase in PD-L1 or HIF-2 α transcription (Extended Data Fig. 3a and b). Moreover, tumor cells obtained from the MCC-133 PDX model consistently confirmed that palbociclib induced an upregulation in the transcription of HIF-2 α and PD-L1 (Fig. 3d and e), providing robust evidence that the activation of HIF-2 α serves as the underlying mechanism for the increased PD-L1 levels. These findings underscore the differential response of MCPyV-positive and -negative MCC cells to palbociclib and its distinct impact on the HIF-2 α /PD-L1 axis.

TC-S7009, a specific inhibitor of HIF-2 α , disrupts HIF-2 α 's heterodimerization and DNA-binding activity, reducing the expression of HIF-2 α -dependent genes (Fig. 3f). Our study explored whether TC-S7009, this HIF-2 α -specific inhibitor, could counteract the palbociclib-induced increase in PD-L1 gene expression in MCC cell lines. Treating WaGa cells with palbociclib led to a time-dependent elevation in PD-L1 expression. However, when co-administered with TC-S7009, PD-L1 transcription was effectively reduced to baseline levels (Fig. 3g). Importantly, this modulation in PD-L1 mRNA expression aligned with changes in PD-L1 protein levels, as illustrated in Extended Data Fig. 4. These findings underscore the promising potential of TC-S7009 in mitigating the palbociclib-induced upregulation of PD-L1.

2.4. The combination of CDK4/6 and HIF-2 α inhibitors can induce the ferroptotic pathway of ICD

Blocking CDK4/6 activity can directly induce cell death by disrupting cellular metabolism, depleting antioxidants, and elevating reactive oxygen species (ROS) levels [61]. This reduction in CDK4/6 activity, primarily dependent on the status of Rb, leads to an increase in ROS, thereby influencing both glycolysis and oxidative metabolism. To investigate the underlying mechanism behind the increase in HIF-2 α levels following palbociclib treatment, we employed a measurement approach targeting hydrogen peroxide (H₂O₂), a representative reactive oxygen species (ROS), using the H₂O₂ biosensor HyPerRed [62], known for its ability to detect H₂O₂ (Fig. 4a). Mitochondria are widely recognized as a significant source of ROS generated during cellular metabolism, and excessive ROS production can overwhelm the cellular antioxidant system, leading to oxidative stress [63]. Among the ROS produced by mitochondria, superoxide and H₂O₂ are the primary contributors. H₂O₂ serves as a central player in redox signaling and oxidative stress modulation [64]. Specific cell lines have been reported to respond to ROS, including H₂O₂, in normoxic conditions, leading to the activation of HIFs. Additionally, treatments aimed at reducing ROS have been shown to mitigate HIF accumulation during hypoxia. In our experimental observations, we noticed a significant increase in HyPerRed signals subsequent to palbociclib treatment (Fig. 4b and c), strongly suggesting that elevated ROS levels were responsible for the upregulation of HIF-2 α . Given that both high ROS levels and heightened HIF-2 α expression can trigger cell death [61], we embarked on investigating whether an HIF-2 α inhibitor could be employed in conjunction with palbociclib. Thus, our study delved into the assessment of cell death in MCC cell lines under various treatment regimens, including sequential and simultaneous exposure to palbociclib and TC-S7009. Interestingly, while co-treatment with the two drugs did not yield additive effects beyond what was achieved individually, the combination treatment exhibited a more potent induction of cell death (Fig. 4d and e). This underscores the potential synergy between the two compounds, presenting a promising avenue for further investigation in cancer therapy.

Through further investigation into the increased cell death, we confirmed the upregulation of the long non-coding RNA (lncRNA) SLC7A11-AS1 [65] after treatment with palbociclib and TC-S7009. lncRNAs, characterized by their extensive nucleotide sequences

exceeding 200 and the absence of protein-coding potential, constitute a class of non-coding RNAs [66]. lncRNAs, which operate in both the nucleus and cytoplasm, play crucial regulatory roles at various levels of gene expression, and among them, a noteworthy subset is the natural antisense transcripts [67]. Indeed, many lncRNAs belong to the category of natural antisense transcripts, which are characterized by RNA sequences transcribed in the opposite direction at the same genomic loci as their corresponding genes [68] and [69]. Nonetheless, the precise biological functions of antisense lncRNAs remain a subject of ongoing investigation and have yet to be fully elucidated. Nevertheless, a growing body of reports has highlighted that lncRNAs can also exert their influence on gene expression through antisense mechanisms. In our current study, we observed that the administration of TC-S7009 to WaGa cells resulted in a more substantial increase in the levels of lncRNA SLC7A11-AS1 compared to treatment with palbociclib alone. Notably, the co-treatment of these compounds significantly enhanced this induction, as shown in Fig. 4f and g. SLC7A11-AS1 is a *cis*-acting natural antisense transcript of the coding gene SLC7A11, located on chromosome 4q28.31 (Fig. 4h). SLC7A11 is a major component of the cysteine-glutamate antiporter, is essential for the uptake of cysteine, and plays a role in intracellular glutathione (GSH) synthesis [70]. Therefore, SLC7A11 is a crucial determinant of cellular redox balance [71]. SLC7A11 tightly regulates lipid peroxidation and prevents non-apoptotic forms of cell death such as ferroptosis [72]. Ferroptosis is caused by the inhibition of cysteine uptake [73]. Reduced cysteine absorption results in fatal lipid ROS such as H₂O₂, and the Fenton reaction of ROS causes membrane lipid peroxide damage due to the accumulation of hydroxyl radicals [74]. Therefore, stable SLC7A11 expression is vital for cell growth and survival [75]. However, annealing of antisense lncRNA SLC7A11-AS1 with SLC7A11 disrupted SLC7A11 activity. As Co-treatment with palbociclib and TC-S7009 sharply increased the level of lncRNA SLC7A11-AS1, and we examined whether this resulted in a reduced level of SLC7A11. qRT-PCR analysis revealed that SLC7A11 was downregulated as the level of SLC7A11-AS1 increased in both WaGa cell lines (Fig. 4i and j), indicating that high levels of the lncRNA SLC7A11-AS1 blocked essential SLC7A11, leading to ferroptosis.

In summary, our study has demonstrated that the CDK4/6 inhibitor palbociclib induces an increase in ROS, specifically H₂O₂, leading to heightened expression of HIF-2 α , which subsequently upregulates the cancer immune checkpoint inhibitor PD-L1. However, the addition of the HIF-2 α inhibitor TC-S7009 effectively counteracts the increase in PD-L1 expression and promotes immunogenic cell death in MCC cells, primarily through ferroptosis. By uncovering this novel mechanism of cell death, our research suggests that a combination therapy approach employing both CDK4/6 and HIF-2 α inhibitors, such as palbociclib and TC-S7009, holds significant promise as an effective strategy against MCC tumors.

3. Discussion

In our study, we explored an innovative combination therapy approach designed to target both the cell cycle and hypoxic responses in aggressive cancers, with a specific emphasis on Merkel cell carcinoma (MCC). Our investigation centered around two essential drugs: Palbociclib, an FDA-approved CDK4/6 inhibitor, and TC-S7009, a HIF-2 α inhibitor. Through our research, we unveiled several notable findings:

First and foremost, we made a pivotal discovery concerning the dynamic regulation of PD-L1 in MCC cells intricately linked to the cell cycle. This observation underscores the importance of considering PD-L1's dynamic regulation during immunotherapy, as it holds significant implications for the outcomes of such treatments.

Furthermore, our study revealed that TC-S7009 effectively countered the palbociclib-induced upregulation of PD-L1. This finding suggests that targeting HIF-2 α with TC-S7009 could serve as a promising strategy to mitigate palbociclib's impact and potentially enhance immunotherapy's effectiveness.

Hypoxia, a condition marked by oxygen deprivation, is known to hinder cell growth during the G1 phase by promoting the activity of CDK inhibitors. However, cancer cells frequently evade these cell division checkpoints through the actions of oxygen-sensitive transcription factors known as hypoxia-inducible factors (HIFs). Heightened HIF activity represents pivotal mechanism cancer cells employ to develop resistance against chemotherapy and radiotherapy. The capability of TC-S7009 to disrupt HIF-2 α activity offers a potential solution to counteract the palbociclib-induced upregulation of PD-L1.

Moreover, our study uncovered a synergistic effect when Palbociclib and TC-S7009 were combined, ultimately leading to Immunogenic Cell Death (ICD) induction. ICD plays a central role in immunotherapy by triggering robust immune responses, facilitating the release of tumor antigens, and modulating the immune system. Additionally, we shed light on the role of ferroptosis, a distinctive form of regulated cell death that differs from apoptosis, as a mechanism contributing to ICD. Ferroptosis stands out due to its origins not in DNA damage but in the accumulation of peroxides in polyunsaturated fatty acid-containing phospholipids (PUFA-PL). This distinct mode of cell death qualifies ferroptosis as a form of ICD, given its capacity to result in the release of HMGB1 and adenosine triphosphate (ATP). Notably, the solute transporter family seven-member 11 (SLC7A11), also known as xCT, plays a critical role as a cystine/glutamate transporter responsible for importing extracellular cystine. Investigating the secretion of calreticulin, HMGB1, and ATP becomes instrumental in identifying novel anticancer drugs capable of inducing ICD. Pursuing an effective combination of cell cycle and hypoxia-related pharmaceutical drugs for ICD holds significant promise in MCC treatment.

Our research underscores the potential of a comprehensive therapeutic strategy that considers dynamic protein regulation in the context of the cell cycle and hypoxia. This approach can significantly enhance the efficacy of immunotherapy and instill optimism for more potent treatments, particularly for aggressive cancers such as MCC.

4. Materials and methods

4.1. Generation of single-cell tumor digests and single-cell RNA sequencing (scRNAseq) & gene expression analysis

Cell Ranger Single-Cell Software Suite (version 2.1.0) was used to perform sample demultiplexing, barcode processing, and single-cell 5'-gene counting. The FASTQ files were processed using the cell ranger *count* pipeline. Reads containing cDNA inserts were aligned to the hg38 human reference genome using STAR [76]. The aligned reads were filtered for valid cell barcodes and unique molecular identifiers (UMIs). Cell barcodes with 1-Hamming-distance from a list of known barcodes were examined. UMIs with a sequencing quality score >10% and no homopolymers were considered valid UMIs. A UMI with a 1-Hamming-distance from another UMI with more reads for the same cell and the same gene was corrected to this UMI with more reads. The default estimated number of cells is 10,000. The Cell Ranger *aggr* pipeline was used to integrate gene-barcode count matrices (from PBMC and tumor samples). Correction of sequencing depth was also performed during aggregation.

The Seurat R package was used for data analysis [77,78]. Library size normalization was performed for each cell type. The UMI counts were divided by the total number of UMI in each cell, followed by multiplication with 10,000 cells. Data were then log-transformed and corrected for unwanted sources of variation, such as the number of detected UMIs using the *ScaleData* R function. The corrected normalized gene-barcode matrix was used as the input to perform PCA. The, and the top ten principal components (PCs) were down selected for clustering. Cell clustering was performed using a graph-based clustering method (*FindNeighbors* and *FindClusters* R functions), with a resolution of 0.8. Visualization in two dimensions (tSNE) was performed using Cloupe.

Differential expression analysis was performed using R package *MAST* [79]. *MAST* provides functionality for the significance testing of differential expression using a hurdle model. It is a two-part generalized linear model that simultaneously models the rate of expression over the background of various transcripts (logistic regression) and positive expression mean (Gaussian). These tests were two-sided and adjusted for the bimodal nature of the single-cell RNA sequencing data. Differential expression analysis was performed between the conditions (tumor and non-tumor). The normalized gene-cell barcode matrix was used as the input, and the model included the cellular detection rate (CDR), defined as the total number of UMIs in a given cell, as a covariate.

4.2. Tissue microarray and Ki-67 staining

TMA slides of 0.6 mm formalin-fixed, paraffin-embedded tumor cores were produced as described previously (6). Triplicate slides containing samples from 31 unique patients was stained for Ki-67. At time of diagnosis, 11 patients (33%) were Stage I, 3 (9.6%) were Stage II, 15 (45%) were Stage III, and 1 (3%) was Stage IV. Four patients had both primary and metastatic lesions included on the TMA. Cores were stained for Ki-67 using MIB-1 antibody (M7240, Dako, Denmark) on a DAKO Autostainer. Antigen retrieval was performed using Dako Citrate Buffer pH 6.0 for 40 min, followed by blocking with TCT buffer. Primary antibody was used at a 1:100 dilution for 60 min, and detection was performed with Biocare Mach2 anti-mouse HRP for 30 min followed by DAB Chromogen. Tonsil cores provided positive controls for Ki-67 staining. Percent Ki-67 positivity was averaged between triplicate samples, and primary and metastatic lesions were considered in cases where both samples were available.

4.3. Cell culture

We used well-described MCC cell lines (MCC13, MS-1, WaGa, MKL-1, and MKL-2), in addition to low-passage cells harvested from MCC-133 patient-derived xenograft (PDX) mice. MCC cell lines were cultured in RPMI medium supplemented with 10% FBS. All cell lines were routinely tested for mycoplasma contamination and negative results were obtained.

4.4. Development of PDX model MCC133 from patient

Needle biopsies of metastasized tumors were collected and frozen in the CryoStor cryogenic medium. The tissue was thawed to 37 °C, rinsed in dPBS, divided into fifths, and embedded in Matrigel (Corning, NY, USA). The matrigel-tumor units were placed subcutaneously into the flanks of five male NSG mice, 6–8 weeks old, under isoflurane anesthesia. Preemptive analgesia was provided using buprenorphine SR 0.50 mg/kg. All animal experiments were approved by the Institutional Animal Care and Use Committee (FHCRC IACUC protocol 50935-200016). Animals were housed under ABSL2 conditions. Four out of five mice had tumors. By day 84, the first mouse developed a palpable tumor, and by day 144 the 4th mouse developed a palpable tumor. Average diameter of tumors at collection was 1.5–1.82 mm, as measured with digital calipers, using formula $(L + W)/2$. The volume of the tumors at collection was 1200–2850 mm³ (>3) and the formula $L*(W^2)/2$ was used. Tumors from the first mouse were divided, half were divided into fifths, and implanted subcutaneously in the second cage of the NSG mice. All five mice in the second passage had tumors. The median time to palpable tumor development in the second passage was 30 days. FFPE blocks from each tumor were administered to the researchers, and the whole tumor tissue was delivered in RPMI on ice to the researchers (within 30 min of collection from mice). Tissue from each tumor was cryopreserved for future use and stored in the PMCL PDX Tumor Bank.

4.5. Patient-derived xenograft

The xenograft was originally established from a needle core biopsy that had been preserved in a Corning Cryostor in LN₂. The tumor was obtained from the passage of the first NSG mouse into the patient tissue.

4.6. Cell-cycle synchronization

HeLa and MCC13 cells were treated with thymidine (Sigma-Aldrich Corp) at a concentration of 2 mM for 16–18 h. The cells were then washed three times with PBS to remove thymidine and cultured in RPMI supplemented with 10% FBS and 1% antibiotics for an additional 8–10 h before the addition of thymidine (2 mM) for 16–18 h. Using this time point as the starting point, the cells were washed with PBS and harvested at the indicated time, 24–40 h.

The double thymidine block procedure was performed as previously described. The harvested cells were fixed with cold ethanol (70%) for flow cytometric cell cycle analysis. Fibroblasts cultured in DMEM supplemented with 10% FBS and 1% antibiotics without any treatment were used as the controls.

The double-thymidine block procedure was performed as previously described. After a second treatment with thymidine (2 mM) for 16–18 h, the cells were washed thrice with PBS to remove thymidine. This time point was designated as 0 h. The cells were treated with 100 ng/mL nocodazole for 4 h at various time intervals after thymidine removal.

4.7. Analysis of cell death using 7-AAD

Following cell culture, treatment, and washing, the cells underwent incubation with the prepared 7-AAD staining solution at the recommended concentration and duration, concluding with a final resuspension step in PBS. Analysis can be done with a flow cytometer, with excitation at around 488 nm and detection in the far-red channel (650–670 nm). Data analysis determines the percentage of cells incorporating 7-AAD, indicating dead or dying cells.

4.8. Flow cytometry analysis

Cells were stained with 0.5 mL PBS containing 40 µg/mL propidium iodide (PI; Sigma) and 0.3 mg/mL RNase A at 37 °C for 30 min. The stained cells were analyzed using a BD Fluorescence-activated cell sorting (FACS) Calibur flow cytometer at 488 nm. For each sample, 20,000 events were recorded and histograms were plotted. The percentage of cells within various phases of the cell cycle was calculated using the FlowJo software (Treestar, Ashland, OR, USA).

4.9. Quantitative real-time PCR

Total RNA was extracted from cells using TRIzol reagent (Invitrogen). After checking RNA purity and concentration, RNA was reverse-transcribed to cDNA using the iScript SuperMix reagent (Bio-Rad). Primers (IDT) were diluted in nuclease-free water using PowerUp SYBR Green Master Mix (Applied Biosystems), and qPCR was performed on an Applied Biosystems 7300 machine. The following primers were used human β -actin: forward, 5' -ACTCTTCCAGCCTTCCTCC- 3', reverse, 5' -CAATGCCAGGGTACATGGTG- 3'; human PD-L1: forward, 5' -GGAAATTCGGCAGTGACC- 3', reverse, 5' -GAAACCTCCAGGAAGCCTCT- 3'; human cMyc: forward, 5' -GAAACCTCCAGGAAGCCTCT- 3', reverse, 5' -TGCGTAGTTGTGCTGATGTG- 3'; human cJun: forward, 5' -CAGGTGGCA-CAGCTTAAACA- 3', reverse, 5' -AACTGCTGCGTTAGCATGAG- 3'; human HIF1A: forward, 5' -TCCAAGAAGCCCTAACGTGT- 3', reverse, 5' -TCCAAGAAGCCCTAACGTGT- 3'; human HIF2A: forward, 5' -AACAGAGGCCGTACTGTCAA- 3', reverse, 5' -GATGGGTGCTGGATTGGTTC- 3'; human RELA: forward, 5' -GGGATGGCTTCTATGAGGCT- 3', reverse, 5' -GGGATGGCTTCTATGAGGCT- 3'; human STAT3: forward, 5' -GAAGGAGGCGTCACTTTTCAC- 3', reverse, 5' -GAAGGAGGCGTCACTTTTCAC- 3'. Relative RNA levels were calculated from the Ct values.

4.10. Western blotting

Cells were synchronized at the G2/M border by thymidine-nocodazole double block, followed by gene and protein expression analyses using qRT-PCR, flow cytometry, and western blotting. Cells were collected and lysed in HEPES buffer (50 mM Tris pH 7.4, 100 mM NaCl, 1% NP-40, 1 mM EDTA) supplemented with protease inhibitors (Roche) and phosphatase inhibitors (Sigma) for western blotting.

4.11. HyPerRed experiment

The level of intracellular H₂O₂ in HyPerRed-expressing cells [62], both control and treated with palbociclib, was analyzed using BD FACSCanto II (BD Biosciences). HyPerRed plasmid was transfected into WaGa cells 24 h before palbociclib treatment. Cells treated with palbociclib were analyzed using flow cytometry after 24 h. As a control, cells were treated with H₂O₂ for 5–10 min.

4.12. Statistical analysis

Each treatment was repeated at least three times. One-way analysis of variance (ANOVA) was used to analyze statistical differences among groups. Statistical significance was set at $P < 0.05$.

CRediT authorship contribution statement

Jung Hyun Lee: Writing - review & editing, Writing - original draft, Validation, Investigation, Formal analysis, Data curation, Conceptualization. **Justin Daho Lee:** Writing - review & editing, Investigation. **Kelly Paulson:** Writing - review & editing, Validation, Investigation, Formal analysis. **Valentin Voillet:** Writing - review & editing, Validation, Software, Investigation, Formal analysis. **Andre Berndt:** Formal analysis. **Candice Church:** Writing - review & editing, Resources. **Kristina Lachance:** Writing - review & editing, Conceptualization. **Song Y. Park:** Writing - review & editing, Investigation, Formal analysis. **Naomi K. Yamamoto:** Writing - review & editing, Formal analysis. **Elizabeth A. Cromwell:** Writing - review & editing, Investigation. **Raphael Gottardo:** Supervision, Software. **Aude G. Chapuis:** Supervision, Resources. **Paul Nghiem:** Writing - review & editing, Writing - original draft, Supervision, Resources, Funding acquisition, Formal analysis, Data curation, Conceptualization.

Declaration of competing interest

The authors declare the following financial interests/personal relationships which may be considered as potential competing interests: Jung Hyun Lee reports financial support and writing assistance were provided by Elsa U. Pardee Foundation.

Acknowledgements

We thank the patients and their families. We also thank Thomas Pulliam for his insightful discussions. We are grateful for SLU flow cytometry facility from University of Washington. This work was supported by the Elsa U. Pardee Foundation, MCC patient gift fund, Preclinical Modeling Core Laboratory Shared Resource of the Fred Hutch/University of Washington Cancer Consortium (P30 CA015704) and NIH (grant P01CA225517).

Appendix A. Supplementary data

Supplementary data to this article can be found online at <https://doi.org/10.1016/j.heliyon.2023.e23521>.

References

- [1] J.C. Becker, A. Stang, J.A. DeCaprio, L. Cerroni, C. Lebbe, M. Veness, P. Nghiem, Merkel cell carcinoma, *Nat. Rev. Dis. Prim.* 3 (2017), 17077.
- [2] R.A. Schmerling, J.G. Casas, G. Cinat, F.E.G. Ospina, L. Kassuga, J.L.M. Tlahuel, L.D. Mazzuoccolo, Burden of disease, early diagnosis, and treatment of Merkel cell carcinoma in Latin America, *J. Glob. Oncol.* 4 (2018) 1–11.
- [3] A. Colunga, T. Pulliam, P. Nghiem, Merkel cell carcinoma in the age of immunotherapy: facts and hopes, *Clin. Cancer Res.* 24 (2018) 2035–2043.
- [4] K.G. Paulson, V. Voillet, M.S. McAfee, D.S. Hunter, F.D. Wagener, M. Perdicchio, W.J. Valente, S.J. Koelle, C.D. Church, N. Vandeven, et al., Acquired cancer resistance to combination immunotherapy from transcriptional loss of class I HLA, *Nat. Commun.* 9 (2018) 3868.
- [5] X. Wu, Z. Gu, Y. Chen, B. Chen, W. Chen, L. Weng, X. Liu, Application of PD-1 blockade in cancer immunotherapy, *Comput. Struct. Biotechnol. J.* 17 (2019) 661–674.
- [6] M.E. Spurgeon, P.F. Lambert, Merkel cell polyomavirus: a newly discovered human virus with oncogenic potential, *Virology* 435 (2013) 118–130.
- [7] M. Malumbres, M. Barbacid, Cell cycle, CDKs and cancer: a changing paradigm, *Nat. Rev. Cancer* 9 (2009) 153–166.
- [8] T. Otto, P. Sicinski, Cell cycle proteins as promising targets in cancer therapy, *Nat. Rev. Cancer* 17 (2017) 93–115.
- [9] J. Massague, G1 cell-cycle control and cancer, *Nature* 432 (2004) 298–306.
- [10] D.O. Morgan, Cyclin-dependent kinases: engines, clocks, and microprocessors, *Annu. Rev. Cell Dev. Biol.* 13 (1997) 261–291.
- [11] J.S. Lim, N.C. Turner, T.A. Yap, CDK4/6 inhibitors: promising opportunities beyond breast cancer, *Cancer Discov.* 6 (2016) 697–699.
- [12] Q. Pan, A. Sathe, P.C. Black, P.J. Goebell, A.M. Kamat, B. Schmitz-Draeger, R. Nawroth, CDK4/6 inhibitors in cancer therapy: a novel treatment strategy for bladder cancer, *Bladder Cancer* 3 (2017) 79–88.
- [13] J. Zhang, X. Bu, H. Wang, Y. Zhu, Y. Geng, N.T. Nihira, Y. Tan, Y. Ci, F. Wu, X. Dai, et al., Cyclin D-CDK4 kinase destabilizes PD-L1 via cullin 3-SPOP to control cancer immune surveillance, *Nature* 553 (2018) 91–95.
- [14] B. Wang, Q. Zhao, Y. Zhang, Z. Liu, Z. Zheng, S. Liu, L. Meng, Y. Xin, X. Jiang, Targeting hypoxia in the tumor microenvironment: a potential strategy to improve cancer immunotherapy, *J. Exp. Clin. Cancer Res.* 40 (2021) 24.
- [15] I. Zerdes, A. Matikas, J. Bergh, G.Z. Rassidakis, T. Foukakis, Genetic, transcriptional and post-translational regulation of the programmed death protein ligand 1 in cancer: biology and clinical correlations, *Oncogene* 37 (2018) 4639–4661.
- [16] Y. Xia, L. Jiang, T. Zhong, The role of HIF-1 α in chemo-/radioresistant tumors, *OncoTargets Ther.* 11 (2018) 3003–3011.
- [17] W. Al Tameemi, T.P. Dale, R.M.K. Al-Jumaily, N.R. Forsyth, Hypoxia-modified cancer cell metabolism, *Front. Cell Dev. Biol.* 7 (2019) 4.
- [18] A. Ahmed, S.W.G. Tait, Targeting immunogenic cell death in cancer, *Mol. Oncol.* 14 (2020) 2994–3006.
- [19] G.L. Semenza, Hypoxia. Cross talk between oxygen sensing and the cell cycle machinery, *Am. J. Physiol. Cell Physiol.* 301 (2011) C550–C552.
- [20] S.H. Baumeister, G.J. Freeman, G. Dranoff, A.H. Sharpe, Coinhibitory pathways in immunotherapy for cancer, *Annu. Rev. Immunol.* 34 (2016) 539–573.
- [21] W. Zou, J.D. Wolchok, L. Chen, PD-L1 (B7-H1) and PD-1 pathway blockade for cancer therapy: mechanisms, response biomarkers, and combinations, *Sci. Transl. Med.* 8 (2016), 328rv324.
- [22] T.R. Cottrell, J.M. Taube, PD-L1 and emerging biomarkers in immune checkpoint blockade therapy, *Cancer J.* 24 (2018) 41–46.
- [23] P.T. Nghiem, S. Bhatia, E.J. Lipson, R.R. Kudchadkar, N.J. Miller, L. Annamalai, S. Berry, E.K. Chertash, A. Daud, S.P. Fling, et al., PD-1 blockade with pembrolizumab in advanced Merkel-cell carcinoma, *N. Engl. J. Med.* 374 (2016) 2542–2552.
- [24] J. Lucas, T.C. Hsieh, H.D. Halicka, Z. Darzynkiewicz, J.M. Wu, Upregulation of PDL1 expression by resveratrol and piceatannol in breast and colorectal cancer cells occurs via HDAC3/p300-mediated NF κ B signaling, *Int. J. Oncol.* 53 (2018) 1469–1480.
- [25] Y. Song, W. Song, Z. Li, W. Song, Y. Wen, J. Li, Q. Xia, M. Zhang, CDC27 promotes tumor progression and affects PD-L1 expression in T-cell lymphoblastic lymphoma, *Front. Oncol.* 10 (2020) 488.
- [26] K.S. Bhullar, N.O. Lagaron, E.M. McGowan, I. Parmar, A. Jha, B.P. Hubbard, H.P.V. Rupasinghe, Kinase-targeted cancer therapies: progress, challenges and future directions, *Mol. Cancer* 17 (2018) 48.
- [27] P. Blume-Jensen, T. Hunter, Oncogenic kinase signalling, *Nature* 411 (2001) 355–365.

- [28] A. Marra, G. Curigliano, Are all cyclin-dependent kinases 4/6 inhibitors created equal? *NPJ Breast Cancer* 5 (2019) 27.
- [29] S. Wedam, L. Fashoyin-Aje, E. Bloomquist, S. Tang, R. Sridhara, K.B. Goldberg, M.R. Theoret, L. Amiri-Kordestani, R. Pazdur, J.A. Beaver, FDA approval summary: palbociclib for male patients with metastatic breast cancer, *Clin. Cancer Res.* 26 (2020) 1208–1212.
- [30] R.S. Herbst, J.C. Soria, M. Kowanetz, G.D. Fine, O. Hamid, M.S. Gordon, J.A. Sosman, D.F. McDermott, J.D. Powderly, S.N. Gettinger, et al., Predictive correlates of response to the anti-PD-L1 antibody MPDL3280A in cancer patients, *Nature* 515 (2014) 563–567.
- [31] M. Lacour, S. Hiltbrunner, S.Y. Lee, A. Soltermann, E.J. Rushing, D. Soldini, W. Weder, A. Curioni-Fontecedro, Adjuvant chemotherapy increases programmed death-ligand 1 (PD-L1) expression in non-small cell lung cancer recurrence, *Clin. Lung Cancer* 20 (2019) 391–396.
- [32] L. Rojko, L. Reiniger, V. Teglas, K. Fabian, O. Pipek, A. Vagvolgyi, L. Agocs, J. Fillinger, Z. Kajdacs, J. Timar, et al., Chemotherapy treatment is associated with altered PD-L1 expression in lung cancer patients, *J. Cancer Res. Clin. Oncol.* 144 (2018) 1219–1226.
- [33] J. Sheng, W. Fang, J. Yu, N. Chen, J. Zhan, Y. Ma, Y. Yang, Y. Huang, H. Zhao, L. Zhang, Expression of programmed death ligand-1 on tumor cells varies pre and post chemotherapy in non-small cell lung cancer, *Sci. Rep.* 6 (2016), 20090.
- [34] V.A. Boussiotis, Molecular and biochemical aspects of the PD-1 checkpoint pathway, *N. Engl. J. Med.* 375 (2016) 1767–1778.
- [35] A.H. Sharpe, K.E. Pauken, The diverse functions of the PD1 inhibitory pathway, *Nat. Rev. Immunol.* 18 (2018) 153–167.
- [36] H. Gonzalez, C. Hagerling, Z. Werb, Roles of the immune system in cancer: from tumor initiation to metastatic progression, *Genes Dev.* 32 (2018) 1267–1284.
- [37] J. Chen, C.C. Jiang, L. Jin, X.D. Zhang, Regulation of PD-L1: a novel role of pro-survival signalling in cancer, *Ann. Oncol.* 27 (2016) 409–416.
- [38] S. Chen, G.A. Crabill, T.S. Pritchard, T.L. McMiller, P. Wei, D.M. Pardoll, F. Pan, S.L. Topalian, Mechanisms regulating PD-L1 expression on tumor and immune cells, *J. Immunother. Cancer* 7 (2019) 305.
- [39] E.M. Rom-Jurek, N. Kirchner, P. Ugocsai, O. Ortmann, A.K. Wege, G. Brockhoff, Regulation of programmed death ligand 1 (PD-L1) expression in breast cancer cell lines in vitro and in immunodeficient and humanized tumor mice, *Int. J. Mol. Sci.* 19 (2018).
- [40] W. Yu, Y. Hua, H. Qiu, J. Hao, K. Zou, Z. Li, S. Hu, P. Guo, M. Chen, S. Sui, et al., PD-L1 promotes tumor growth and progression by activating WIP and beta-catenin signaling pathways and predicts poor prognosis in lung cancer, *Cell Death Dis.* 11 (2020) 506.
- [41] N. Fischer, J. Brandner, F. Fuchs, I. Moll, A. Grundhoff, Detection of Merkel cell polyomavirus (MCPyV) in Merkel cell carcinoma cell lines: cell morphology and growth phenotype do not reflect presence of the virus, *Int. J. Cancer* 126 (2010) 2133–2142.
- [42] J.A. DeCaprio, Merkel cell polyomavirus and Merkel cell carcinoma, *Philos. Trans. R. Soc. Lond. B Biol. Sci.* 372 (2017).
- [43] W. Liu, M. MacDonald, J. You, Merkel cell polyomavirus infection and Merkel cell carcinoma, *Curr Opin Virol* 20 (2016) 20–27.
- [44] C.F. Baez, R. Brandao Varella, S. Villani, S. Delbue, Human polyomaviruses: the battle of large and small tumor antigens, *Virology* 8 (2017), 1178122X17744785.
- [45] V. Pietropaolo, C. Prezioso, U. Moens, Merkel cell polyomavirus and Merkel cell carcinoma, *Cancers* 12 (2020).
- [46] J.C.M. Prado, T.A. Monezi, A.T. Amorim, V. Lino, A. Paladino, E. Boccardo, Human polyomaviruses and cancer: an overview, *Clinics (Sao Paulo)* 73 (2018) e558s.
- [47] S. Borchert, M. Czech-Sioli, F. Neumann, C. Schmidt, P. Wimmer, T. Dobner, A. Grundhoff, N. Fischer, High-affinity Rb binding, p53 inhibition, subcellular localization, and transformation by wild-type or tumor-derived shortened Merkel cell polyomavirus large T antigens, *J. Virol.* 88 (2014) 3144–3160.
- [48] S. Hesbacher, L. Pfitzer, S. Angermeyer, A. Borst, S. Haferkamp, C.J. Scholz, M. Wobser, D. Schrama, R. Houben, RB1 is the crucial target of the Merkel cell polyomavirus Large T antigen in Merkel cell carcinoma cells, *Oncotarget* 7 (2016) 32956–32968.
- [49] I. Schmid, C.H. Uittenbogaart, J.V. Giorgi, Sensitive method for measuring apoptosis and cell surface phenotype in human thymocytes by flow cytometry, *Cytometry* 15 (1994) 12–20.
- [50] X. Shen, L. Zhang, J. Li, Y. Li, Y. Wang, Z.X. Xu, Recent findings in the regulation of programmed death ligand 1 expression, *Front. Immunol.* 10 (2019) 1337.
- [51] C. Sun, R. Mezzadra, T.N. Schumacher, Regulation and function of the PD-L1 checkpoint, *Immunity* 48 (2018) 434–452.
- [52] P. Ritprajak, M. Azuma, Intrinsic and extrinsic control of expression of the immunoregulatory molecule PD-L1 in epithelial cells and squamous cell carcinoma, *Oral Oncol.* 51 (2015) 221–228.
- [53] Y. Wang, H. Wang, H. Yao, C. Li, J.Y. Fang, J. Xu, Regulation of PD-L1: emerging routes for targeting tumor immune evasion, *Front. Pharmacol.* 9 (2018) 536.
- [54] H.Y. Ng, J. Li, L. Tao, A.K. Lam, K.W. Chan, J.M.Y. Ko, V.Z. Yu, M. Wong, B. Li, M.L. Lung, Chemotherapeutic treatments increase PD-L1 expression in esophageal squamous cell carcinoma through EGFR/ERK activation, *Transl. Oncol.* 11 (2018) 1323–1333.
- [55] J.M. Hsu, C.W. Li, Y.J. Lai, M.C. Hung, Posttranslational modifications of PD-L1 and their applications in cancer therapy, *Cancer Res.* 78 (2018) 6349–6353.
- [56] C.W. Li, S.O. Lim, W. Xia, H.H. Lee, L.C. Chan, C.W. Kuo, K.H. Khoo, S.S. Chang, J.H. Cha, T. Kim, et al., Glycosylation and stabilization of programmed death ligand-1 suppresses T-cell activity, *Nat. Commun.* 7 (2016), 12632.
- [57] A.A. Davis, V.G. Patel, The role of PD-L1 expression as a predictive biomarker: an analysis of all US Food and Drug Administration (FDA) approvals of immune checkpoint inhibitors, *J. Immunother. Cancer* 7 (2019) 278.
- [58] A. Ribas, S. Hu-Lieskovan, What does PD-L1 positive or negative mean? *J. Exp. Med.* 213 (2016) 2835–2840.
- [59] C. Travert, F. Barlesi, L. Greillier, P. Tomasini, Immune oncology biomarkers in lung cancer: an overview, *Curr. Oncol. Rep.* 22 (2020) 107.
- [60] S.C. Casey, L. Tong, Y. Li, R. Do, S. Walz, K.N. Fitzgerald, A.M. Gouw, V. Baylot, I. Gutgemann, M. Eilers, et al., MYC regulates the antitumor immune response through CD47 and PD-L1, *Science* 352 (2016) 227–231.
- [61] J. Franco, U. Balaji, E. Freinkman, A.K. Witkiewicz, E.S. Knudsen, Metabolic reprogramming of pancreatic cancer mediated by CDK4/6 inhibition elicits unique vulnerabilities, *Cell Rep.* 14 (2016) 979–990.
- [62] Y.G. Ermakova, D.S. Bilan, M.E. Matlashov, N.M. Mishina, K.N. Markvicheva, O.M. Subach, F.V. Subach, I. Bogeski, M. Hoth, G. Enikolopov, et al., Red fluorescent genetically encoded indicator for intracellular hydrogen peroxide, *Nat. Commun.* 5 (2014) 5222.
- [63] J. Dan Dunn, L.A. Alvarez, X. Zhang, T. Soldati, Reactive oxygen species and mitochondria: a nexus of cellular homeostasis, *Redox Biol.* 6 (2015) 472–485.
- [64] H. Sies, Hydrogen peroxide as a central redox signaling molecule in physiological oxidative stress: oxidative eustress, *Redox Biol.* 11 (2017) 613–619.
- [65] Y. Luo, C. Wang, P. Yong, P. Ye, Z. Liu, Z. Fu, F. Lu, W. Xiang, W. Tan, J. Xiao, Decreased expression of the long non-coding RNA SLC7A11-AS1 predicts poor prognosis and promotes tumor growth in gastric cancer, *Oncotarget* 8 (2017) 112530–112549.
- [66] J.T. Kung, D. Colognori, J.T. Lee, Long noncoding RNAs: past, present, and future, *Genetics* 193 (2013) 651–669.
- [67] X. Dai, A.C. Kaushik, J. Zhang, The emerging role of major regulatory RNAs in cancer control, *Front. Oncol.* 9 (2019) 920.
- [68] M. Jadalila, O. Gholamalamdari, W. Tang, Y. Zhang, A. Petracovici, Q. Hao, A. Tariq, T.G. Kim, S.E. Holton, D.K. Singh, et al., A natural antisense lncRNA controls breast cancer progression by promoting tumor suppressor gene mRNA stability, *PLoS Genet.* 14 (2018), e1007802.
- [69] J.C.R. Fernandes, S.M. Acuna, J.I. Aoki, L.M. Floeter-Winter, S.M. Muxel, Long non-coding RNAs in the regulation of gene expression: physiology and disease, *Noncoding RNA* 5 (2019).
- [70] J. Lewerenz, S.J. Hewett, Y. Huang, M. Lambros, P.W. Gout, P.W. Kalivas, A. Massie, I. Smolders, A. Methner, M. Pergande, et al., The cystine/glutamate antiporter system x(c)(-) in health and disease: from molecular mechanisms to novel therapeutic opportunities, *Antioxidants Redox Signal.* 18 (2013) 522–555.
- [71] J.K.M. Lim, A. Delaidelli, S.W. Minaker, H.F. Zhang, M. Colovic, H. Yang, G.L. Negri, S. von Karstedt, W.W. Lockwood, P. Schaffer, et al., Cystine/glutamate antiporter xCT (SLC7A11) facilitates oncogenic RAS transformation by preserving intracellular redox balance, *Proc. Natl. Acad. Sci. U. S. A.* 116 (2019) 9433–9442.
- [72] B.R. Stockwell, J.P. Friedmann Angeli, H. Bayir, A.I. Bush, M. Conrad, S.J. Dixon, S. Fulda, S. Gascon, S.K. Hatzios, V.E. Kagan, et al., Ferroptosis: a regulated cell death nexus linking metabolism, redox biology, and disease, *Cell* 171 (2017) 273–285.
- [73] S. Hao, B. Liang, Q. Huang, S. Dong, Z. Wu, W. He, M. Shi, Metabolic networks in ferroptosis, *Oncol. Lett.* 15 (2018) 5405–5411.
- [74] N. Kajarabille, G.O. Latunde-Dada, Programmed cell-death by ferroptosis: antioxidants as mitigators, *Int. J. Mol. Sci.* 20 (2019).
- [75] P. Koppula, Y. Zhang, L. Zhuang, B. Gan, Amino acid transporter SLC7A11/xCT at the crossroads of regulating redox homeostasis and nutrient dependency of cancer, *Cancer Commun.* 38 (2018) 12.
- [76] A. Dobin, C.A. Davis, F. Schlesinger, J. Drenkow, C. Zaleski, S. Jha, P. Batut, M. Chaisson, T.R. Gingeras, STAR: ultrafast universal RNA-seq aligner, *Bioinformatics* 29 (2013) 15–21.

- [77] A. Butler, P. Hoffman, P. Smibert, E. Papalexi, R. Satija, Integrating single-cell transcriptomic data across different conditions, technologies, and species, *Nat. Biotechnol.* 36 (2018) 411–420.
- [78] T. Stuart, A. Butler, P. Hoffman, C. Hafemeister, E. Papalexi, W.M. Mauck 3rd, Y. Hao, M. Stoeckius, P. Smibert, R. Satija, Comprehensive integration of single-cell data, *Cell* 177 (2019) 1888–1902 e1821.
- [79] G. Finak, A. McDavid, M. Yajima, J. Deng, V. Gersuk, A.K. Shalek, C.K. Slichter, H.W. Miller, M.J. McElrath, M. Prlic, et al., MAST: a flexible statistical framework for assessing transcriptional changes and characterizing heterogeneity in single-cell RNA sequencing data, *Genome Biol.* 16 (2015) 278.